11-26-2013

Wave Heating and Jeans Escape in the Martian Upper Atmosphere

R. L. Walterscheid
The Aerospace Corporation

Michael P. Hickey Ph.D.
Embry-Riddle Aeronautical University, hicke0b5@erau.edu

G. Schubert
Institute of Geophysics and Planetary Physics, University of California

Scholarly Commons Citation

Walterscheid, R. L., M. P. Hickey, and G. Schubert (2013), Wave heating and Jeans escape in the Martian upper atmosphere, J. Geophys. Res. Planets, 118, 2413–2422, doi: https://doi.org/10.1002/jgre.20164

Wave heating and Jeans escape in the Martian upper atmosphere

R. L. Walterscheid,[1] M. P. Hickey,[2] and G. Schubert[3]

Received 27 March 2013; revised 18 September 2013; accepted 28 September 2013; published 26 November 2013.

[1] Gusty flow over rough terrain is likely to be a significant source of fast gravity waves and acoustic waves in the atmosphere of Mars, as it is in Earth's atmosphere. Accordingly, we have used a numerical model to study the dissipation in the thermosphere and exosphere of Mars of upward-propagating fast gravity waves and acoustic waves. Model simulations are performed for a range of wave periods and horizontal wavelengths. Wave amplitudes are constrained by the Mars Global Surveyor and Mars Odyssey aerobraking data, and gravity wave phase velocities are limited by occultation data. Dissipating gravity waves heat some regions of the thermosphere and cool others through the effects of sensible heat flux divergence, while acoustic waves mainly heat the Mars thermosphere. Heating rates can be on the order of several hundred Kelvin per day. The cycle-integrated effects on the Jeans escape flux are also investigated and found to be on the order of background values and even greater and might be a significant source of loss of the Martian atmosphere to space.

Citation: Walterscheid, R. L., M. P. Hickey, and G. Schubert (2013), Wave heating and Jeans escape in the Martian upper atmosphere, *J. Geophys. Res. Planets*, *118*, 2413–2422, doi:10.1002/jgre.20164.

1. Introduction

[2] There is a growing body of evidence for the widespread and frequent occurrence of gravity waves in the Martian atmosphere and for their importance in affecting the state of the upper atmosphere [*Medvedev et al*., 2011; *Spiga et al*., 2012; *Miyoshi et al*., 2011; *Parish et al*., 2009; *Forget et al*., 2009; *Fritts et al*., 2006; *Ando et al*., 2012; *Creasey et al*., 2006a, 2006b]. Wavelike density and temperature variations are seen in stellar occultation profiles in the upper atmosphere [*Forget et al*., 2009]. Large variances in density occur along quasi-horizontal tracks observed during aerobraking in the lower thermosphere [*Fritts et al*., 2006]. Large wave-induced thermal effects in the Mars thermosphere related to changes in the background shear caused by wave drag have been simulated by *Medvedev et al*. [2011]. *Medvedev and Yigit* [2012] parameterized the effects of sensible heat fluxes induced by gravity waves and found a significant cooling (up to 45 K) in the middle to high latitude upper mesosphere and lower thermosphere during winter.

[3] Gravity wave energy in the Martian lower atmosphere peaks in mountainous regions, and this behavior indicates that the wave source is orographic in nature [*Medvedev et al*., 2011]. *Creasey et al*. [2006a] found that gravity wave activity in the lower atmosphere correlates well with topography in some but not all cases. Curiously, accelerometer data show little correlation at lower thermospheric altitudes with the underlying topography *Creasey et al*. [2006a]. Perhaps this is related to the filtering of slower gravity waves generated by steep terrain and the more extensive regions of hilly terrain that may serve as sources for fast gravity and acoustic waves [*Walterscheid and Hickey*, 2005].

[4] Modeling suggests that cold pockets in the upper mesosphere are associated with orographically generated waves [*Spiga et al*., 2012]. Waves with nonzero phase speed may contribute as well [*Medvedev et al*., 2011]. Gusty flow over rough terrain in the Earth's troposphere generates fast gravity waves and acoustic waves [*Walterscheid and Hickey*, 2005] that propagate upward into the Earth's thermosphere and heat it by the wave transport of sensible heat and molecular dissipation [*Walterscheid*, 1981; *Hickey et al*., 2001]. Mars has large areas of high terrain with large slopes at typical gravity and acoustic wave scales and gusty surface winds [*Aharonson et al*., 2001; *Lewis et al*., 1999; *Fenton and Michaels*, 2010; *Leovy*, 2001] which should launch fast waves that travel into the Mars upper atmosphere. Some of these waves will heat Mars' upper atmosphere and, as we will show, induce a cycle- averaged Jeans escape flux. Gravity waves can also cool the upper Mars thermosphere through the effects of sensible heat flux divergence [*Walterscheid*, 1981; *Hickey et al*., 2000]. In the case of the upper atmospheres of Earth and Jupiter, dissipating acoustic waves heat the thermosphere [*Hickey et al*., 2001; *Schubert et al*., 2003]. We will determine if the same holds true for gravity and acoustic waves dissipating in Mars upper atmosphere.

2. Model

[5] A full-wave model that solves the complete linearized equations of continuity, momentum, and energy for a compressible, viscous, and thermally conducting atmosphere

[1]Space Science Applications Laboratory, The Aerospace Corporation, Los Angeles, California, USA.
[2]Department of Physical Sciences, Embry-Riddle Aeronautical University, Daytona Beach, Florida, USA.
[3]Department of Earth, Planetary, and Space Sciences, University of California, Los Angeles, California, USA.

Corresponding author: R. L. Walterscheid, Space Science Applications Laboratory, The Aerospace Corporation, Los Angeles, CA 90009, USA. (richard.walterscheid@aero.org)

2169-9097/13/10.1002/jgre.20164

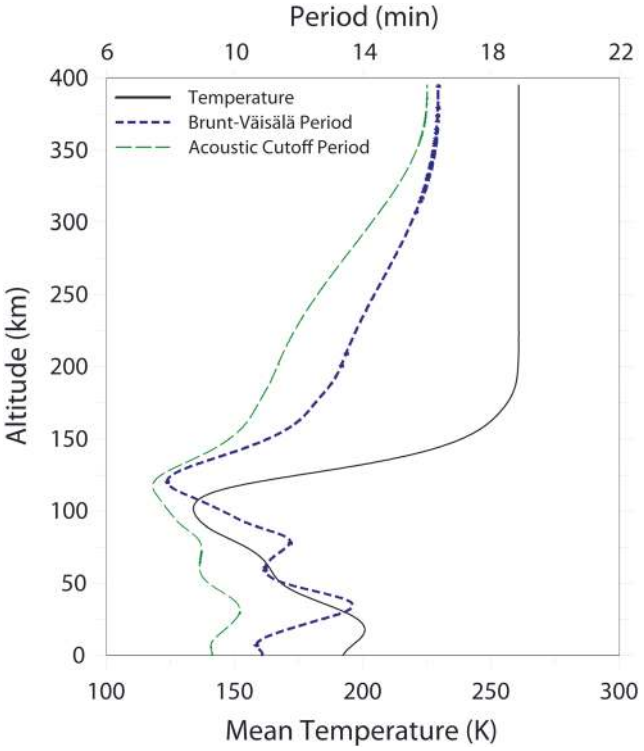

Figure 1. Basic state altitude profiles of temperature, Brunt-Väisälä period, and acoustic cutoff period.

with arbitrary altitude variation in basic state thermal structure is used to calculate the upward propagation of gravity and acoustic waves in the Martian atmosphere. The linearized equations are given in *Schubert et al*. [2003]. A full-wave model, unlike a Wentzel-Kramers-Brillouin model, rigorously accounts for wave reflection. Details of the model and its application to the upward propagation of gravity waves in the atmospheres of Jupiter and Earth can be found in *Hickey et al*. [2000], *Walterscheid and Hickey* [2001], and *Schubert et al*. [2003]. The model domain extends from the surface to altitudes as high as 400 km. The upper boundary height depends on the particular wave being simulated. The radiation condition is applied at the upper boundary.

[6] A sponge layer applied at the top of the model domain insures against spurious wave reflections from the upper boundary. Damping is applied in both the momentum and energy equations. The expression for the Rayleigh friction coefficient K_R is

$$K_R = \omega e^{(z-z_u)/H_u} \tag{1}$$

where ω is the wave frequency, subscript u refers to the sponge layers values, z is altitude, and H is a damping-scale height. In all calculations, $H_u = 40$ km and z_u is equal to the upper boundary height. The Newtonian cooling coefficient in the sponge layer is taken equal to the Rayleigh friction coefficient.

[7] Below the sponge layer damping is by viscosity only. We consider only nonbreaking waves. Damping has a minimal effect on wave amplitude when $\omega/\sigma >> 1$, where ω is the wave frequency and σ is the damping rate (the inverse of the damping time scale). With respect to radiative damping, the results of *Eckermann et al*. [2011] indicate $\omega/\sigma >> 1$. The viscous time scale is $\sigma \sim m^2 \nu$, where m is the vertical wave number and ν is the kinematic viscosity [*Walterscheid and Hickey*, 2011]. The waves we consider are all fast waves with fairly long vertical wavelengths, and they do not experience significant viscous dissipation until they attain lower thermospheric altitudes and higher.

[8] The waves are forced at the ground ($z = 0$) via a specified boundary condition imposed on the vertical velocity w'.

3. Model Parameters

[9] Mean state quantities needed in our computations are the same as those used in *Parish et al*. [2009]. The zonally averaged undisturbed mean state atmosphere for Mars is provided by the Laboratoire de Météorologie Dynamique (LMD) general circulation model [*Forget et al*., 1999; *Angelats i Coll et al*., 2005]. The mean state conditions adopted here are for LS270, northern hemisphere winter solstice, and latitude 45°N. The mean state in the full-wave model simulations is assumed not to vary in time or in the horizontal direction.

[10] The mean temperature and the associated Brunt-Väisälä and acoustic cutoff periods are shown in Figure 1 for 45°N. Both Brunt-Väisälä and acoustic cutoff periods are evaluated by taking into account the variations of temperature and mean molecular weight with height [*Walterscheid and Hecht*, 2003; *Walterscheid and Hickey*, 2001, 2005]. The temperature (solid curve) increases from the minimum at the mesopause (~110 km) to a constant with a value of around 260 K above ~160 km. Minima in the Brunt-Väisälä period are located near 10, 60, and 125 km with maxima near 35 and 80 km. Values increase monotonically above the uppermost minimum. Increasing values in the isothermal upper thermosphere reflect the change in composition from primarily CO_2 in the lower atmosphere to largely O in the upper thermosphere [*Parish et al*., 2009]. The acoustic cutoff period is less than the Brunt-Väisälä period, but it shows similar features.

[11] The values of atmospheric parameters simulated by the LMD model have been validated in comparison with observations. In particular, the simulated Mars temperature profile is found to compare favorably with entry temperature profiles from Mars Pathfinder and the two Viking landers [*Lewis et al*., 1999]. The coefficients of molecular viscosity and thermal conductivity for the background atmosphere are provided by the LMD model [*Parish et al*., 2009]. Eddy momentum diffusivity is based on values from the Viking spacecraft [*Izakov*, 1978]. Eddy thermal diffusivity is calculated from the eddy momentum diffusivity, assuming a Prandtl number of 2, based on values estimated for the Earth [*Fritts and Dunkerton*, 1985; *Strobel*, 1989].

[12] The variations with altitude of mean molecular weight M and sound speed c_S with altitude are shown in Figure 2. Note the steep gradient in mean molecular weight between ~150 and 250 km as the dominant species changes from carbon dioxide to atomic oxygen. This is reflected in the static stability.

[13] All gravity waves are evanescent for $\omega > N$ where ω is wave frequency and N is the Brunt-Väisälä frequency. All acoustic waves are evanescent for $\omega < \omega_a$ where ω_a is the acoustic cutoff frequency. Likewise, acoustic waves are evanescent when $c < c_s$, where c is phase speed and c_s is

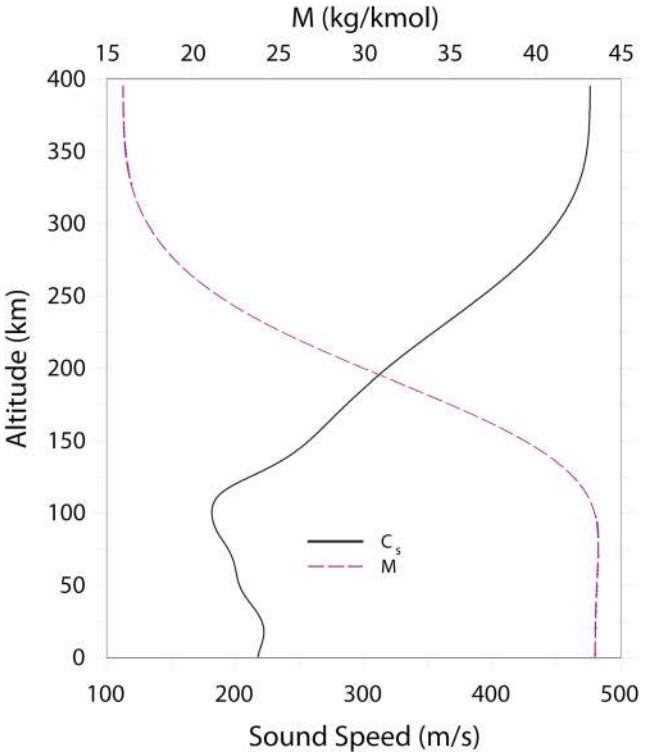

Figure 2. Altitude profiles of basic state sound speed c_s and mean molecular weight M.

sound speed. For gravity waves to propagate from the troposphere (where they are likely generated) to the thermosphere, the period must exceed ~14 min. For sound waves, the period must be less than ~8 min. For acoustic waves to attain altitudes a few scale heights above the mesopause with significant amplitude, the phase speed must exceed ~200 m s^{-1}; to attain altitudes high in the exosphere, it must exceed ~400 m s^{-1}.

[14] We will consider the upward propagation of fast gravity waves and acoustic waves whose periods, horizontal wavelengths, and horizontal phase velocities are summarized in Table 1. The periods were chosen to span a large range of acoustic wave frequencies and wave numbers in the infrasonic region and a range of fast gravity waves. The phase speed for gravity waves was chosen to be consistent with the wavelengths inferred for the stratosphere by *Ando et al*. [2012].

[15] Amplitudes for all waves were chosen to be consistent with the Mars Global Surveyor and Mars Odyssey accelerometer data, giving mass density fluctuation amplitudes at altitudes near 125 km. The mean amplitude of these fluctuations was large, on the order of 25% of the background state [*Fritts et al*., 2006]. Fluctuations of this order are inconsistent with a spectrum strongly dominated by slow gravity waves since these waves would far exceed the breakdown level [*Orlanski and Bryan*, 1969; *Walterscheid and Schubert*, 1990]. We subdivide the spectrum between the waves to be consistent with amplitude spectra having power spectral slopes of −2 for frequency and wave number. This is done by subdividing the spectrum into finite intervals that increase in width as a power of two with increasing frequency and wave number and then assigning the same amplitude to each. Slopes of −2 are roughly consistent with terrestrial observations of gravity waves [*Hecht et al*., 1995; *VanZandt*, 1982].

[16] The spectral slope for acoustic waves in the upper atmosphere is not known, but most likely, the waves in the infrasonic range should have the greatest amplitudes with slower waves dominating [*Walterscheid et al*., 2003]. Thus, spectral intervals defined in this way contribute roughly equal amounts to the root-mean-square wave amplitude. Subdividing in this way also gives a ω, k spectrum that represents a large sector of the internal wave spectrum for both acoustic and gravity waves. To add an additional measure of conservatism, we divide the amplitudes observed by *Fritts et al*. [2006] by a factor of 10, giving a relative density amplitude near 125 km of 2.5% for each wave. We normalize the forcing amplitude to give this wave amplitude at 125 km.

[17] The nominal set of acoustic waves is denoted Set 1. The acoustic waves in this set peak in the upper thermosphere and lower exosphere. The gravity waves peak in the lower thermosphere. We will examine wave propagation and heating rates for these waves. We will also examine the heating rates for faster acoustic and gravity waves that reach greater altitudes. This set is denoted Set 2.

[18] Calculations were also performed for acoustic waves with phase speeds of 200 m s^{-1}. As expected, the waves are strongly attenuated at altitudes above ~120 km.

4. Wave Heating and Cooling

[19] Waves heat or cool the background atmosphere at the rate Q. (degrees per unit time) given to second order by *Hickey et al*. [2000]

$$\bar{\rho} c_p Q = \left\langle \underline{\underline{\sigma}}' : \underline{\nabla}\, \underline{v}' \right\rangle - \frac{d}{dz}\left\{ c_p \bar{\rho} \langle w' T' \rangle \right\} + \left\langle \underline{v}' \cdot \nabla p' \right\rangle - \frac{d\bar{p}}{dz} \frac{\langle w' \rho' \rangle}{\bar{\rho}} \tag{2}$$

[20] In (2), the angle brackets denote an x, y, t average (x and y are horizontal Cartesian coordinates, and t is time), z is altitude, T' is wave temperature perturbation, $\underline{v}'$ is the wave

Table 1. Gravity and Acoustic Wave Parameters Used in the Calculations

Period (min)	Horizontal Wavelength (km)	Horizontal Phase Speed (m s^{-1})
	Acoustic Waves (*Set 1*)	
0.5	9	300
1	18	300
2	36	300
4	72	300
8	144	300
	Gravity Waves (*Set 1*)	
16	48	50
32	96	50
	Acoustic Waves (*Set 2*)	
0.5	12	400
1	24	400
2	48	400
4	96	400
8	192	400
	Gravity Waves (*Set 2*)	
32	288	150

velocity vector, $\underline{\underline{\sigma}}'$ is the molecular viscous stress tensor of the wave field, c_p is the specific heat at constant pressure, ρ is density, w is vertical velocity, p is pressure, primes refer to wave quantities, and overbars refer to basic state quantities. In (2), the first term on the right side is the heating rate due to viscous dissipation of wave kinetic energy (designated $\overline{\rho} c_p Q_{\mathrm{vis}}$). The second term on the right side of (2) is the sensible heat flux divergence [*Walterscheid*, 1981] (designated $\overline{\rho} c_p Q_{w'T'}$). The third term on the right side of (2) is the work done per unit time by the wave-induced pressure gradients (designated $\overline{\rho} c_p \; Q_{v' \mathrm{grad} p'}$). The fourth term on the right of (2) represents the work done per unit time by the second-order wave-induced Eulerian drift in transporting mass in the gravitational field (designated $\overline{\rho} c_p \; Q_{w'\rho'}$). In writing (2) we have ignored dissipation due to eddy viscosity since eddy viscosity is small compared with molecular viscosity at the thermospheric altitudes where the waves dissipate. In most instances the total wave-induced heating is dominated by the sensible heat flux [*Hickey et al*., 2011].

5. Jeans Escape

5.1. Atmospheric Escape Mechanisms

[21] The Martian upper atmosphere escapes to space through a number of different mechanisms. The relative importance of the various escape mechanisms is not well understood. Indeed, a prime objective of NASA's MAVEN mission is to obtain quantitative estimates of the escape rates for the different processes. However, the results of this paper show that Jeans escape can be strongly enhanced by acoustic-gravity waves that reach the upper atmosphere. Here we briefly mention the escape mechanisms that might be important (see the review by *Johnson et al*. [2008]).

5.1.1. Jeans Escape

[22] Jeans escape is a thermal loss mechanism involving neutral species at and above the exobase whose velocities exceed the escape velocity (5 km s^{-1}) from Mars. If these species are moving in the upward direction at the exobase, they will not suffer any collisions and thus they can be lost to space [*Jeans*, 1925]. This effectively defines the exobase, the lower boundary of the exosphere.

5.1.2. Photochemical Loss

[23] Escape is like Jeans escape except that the energetic atoms are produced photochemically and are not simply part of the tail of a thermal distribution.

5.1.3. Ion Pickup and Sputtering

[24] Ion pickup occurs mainly on the Sun-facing hemisphere of Mars where the solar wind impinges directly on the upper atmosphere. Ions are created by photoionization, electron impact ionization, and charge exchange. Most of the pickup ions are accelerated over the planet's poles (for a typical solar wind magnetic field) and are lost down the wake. Some pickup ions have trajectories that impact the atmosphere with sufficient energy to impart escape velocity to exospheric neutrals by collisions, a process called atmospheric sputtering.

5.1.4. Solar Energetic Particles

[25] Solar energetic particles are accelerated by solar flares and associated fast coronal mass ejections to much higher energies (10 s of keV to > ~100 s of MeV) than pickup ions. They produce sputtering, heating, and ionization effects similar to those by pickup ions, but extending much deeper into the atmosphere.

5.1.5. Ion Bulk Escape

[26] Ion bulk escape occurs when momentum transfer from the impinging solar wind strips off coherent blobs of plasma from the ionosphere. The detached clouds of ions and electrons are carried downstream by the solar wind, analogous to the detached tail of a comet, and lost.

5.1.6. Ion Outflow

[27] Ion outflow is the direct outflow of planetary ions to space on open magnetic field lines that connect to interplanetary field lines. Outflow is driven by outward-directed electric fields and by ion heating. On Mars the loops formed by remnant crustal magnetic fields will connect at times with the interplanetary magnetic field lines, forming cusps and open magnetic field lines along which ions can flow outward.

5.2. Wave-Induced Jeans Escape

[28] Here we derive the perturbed Jeans escape due to the effects of heating. The effects of winds should also be considered in a full treatment, but they are very complex and beyond the scope of this paper [*Hartle and Mayr*, 1976]. The formula for the Jeans escape flux in molecules per unit area and per unit time neglecting winds is

$$\phi = NA(1+\lambda)e^{-\lambda} \tag{3}$$

[*Jeans*, 1925] where

$$A = (C_A T)^{\frac{1}{2}} \tag{4}$$

$$\lambda = C_\lambda / T \tag{5}$$

and where N is total number density, $A = \sqrt{kT/2\pi m}$, $\lambda = GMm/kTR_c$, whence $C_A = k/2\pi m$ and $C_\lambda = GMm/kR_c$. Here k is Boltzmann's constant, T is temperature at the exobase, m is the molecular mass, G is the gravitational constant, M is the planetary mass, and R_c is the radius at the height of the exobase. At the exobase altitude (219 km), values of C_A and C_λ are 49.5 m^{2}s^{-2}K^{-1} and 4.3×10^4 K, respectively.

It is convenient to use the log form

$$\log \phi = \log N + \log A + \log(1+\lambda) - \lambda \tag{6}$$

whence

$$\log \phi = \log\left[\overline{N}\left(1+\frac{N'}{\overline{N}}\right)\right] + \frac{1}{2}\log\left[\overline{A}\left(1+\frac{A'}{\overline{A}}\right)\right] + \log\left[(1+\overline{\lambda})\left(1+\frac{\lambda'}{1+\overline{\lambda}}\right)\right] - \left[\lambda' + \overline{\lambda}\right] \tag{7}$$

Subtracting off the wave-undisturbed part gives

$$\log\left(1+\frac{\phi'}{\overline{\phi}}\right) = \log\left(1+\frac{N'}{\overline{N}}\right) + \log\left(1+\frac{A'}{\overline{A}}\right) + \log\left(1+\frac{\lambda'}{1+\overline{\lambda}}\right) - \lambda' \tag{8}$$

and

$$\frac{\phi'}{\overline{\phi}} = \left(1+\frac{N'}{\overline{N}}\right)\left(1+\frac{A'}{\overline{A}}\right)\left(1+\frac{\lambda'}{1+\overline{\lambda}}\right)e^{-\lambda'} - 1 \tag{9}$$

To evaluate (9) in terms of temperature, one needs

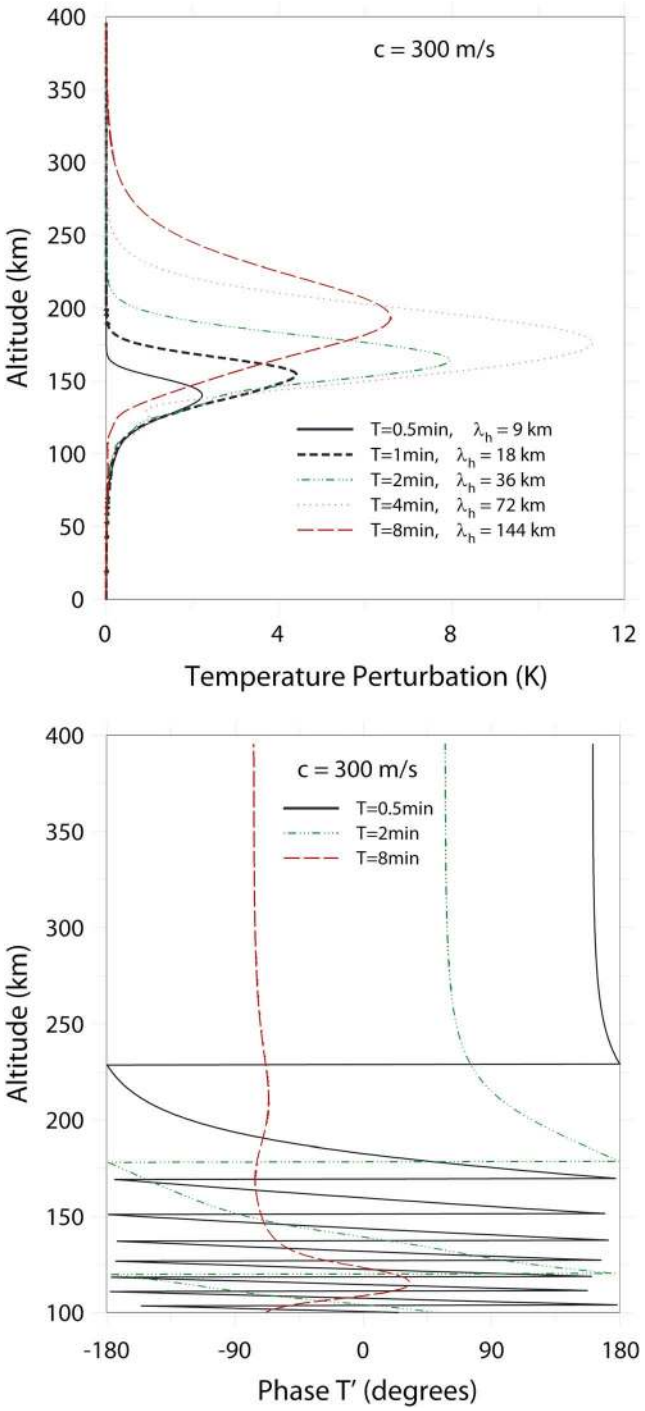

Figure 3. Amplitude of T' versus altitude for the five Set1 acoustic waves listed in Table 1.

$$A' = (C_A T)^{\frac{1}{2}} - \left(C_A \overline{T}\right)^{\frac{1}{2}} \tag{10}$$

$$\lambda' = C_\lambda / T - C_\lambda / \overline{T} \tag{11}$$

6. Results

[29] Figure 3a shows altitude profiles of the amplitude and phase of the temperature perturbation for the five Set 1 acoustic waves whose properties are listed in Table 1. The phases are shown in Figure 3b, where only three waves are shown for clarity. The longer period waves propagate progressively higher before they are attenuated by a combination of evanescence and viscosity and thermal conduction. The feature in the phase variation near 120 km for the 8 min wave is due to the proximity of the wave frequency to the acoustic cutoff frequency. The phase speed for these waves is equal to the sound speed near 200 km, and no wave in the set propagates above this level to a significant extent. Above ~200 km the phase variations of all waves exhibit evanescence modified by viscous dissipation, which induces a real (propagating) component for waves that would otherwise be purely evanescent (and exhibit constant phase). The largest temperature amplitude is 11 K for the 4 min wave, peaking near 180 km. The smallest amplitude is 2 K for the 30 s wave. It is the lowest peaking wave, with the peak found near 140 K. The peak altitudes for each acoustic wave and the corresponding value of T' are given in Table 2.

[30] Figure 4a shows altitude profiles of the amplitude and phase of the temperature perturbation for the two Set 1 gravity waves listed in Table 1. These waves peak in the lower thermosphere and produce both heating and cooling. The 32 min wave peaks near 130 km, with the 16 min wave peaking somewhat higher. The amplitude of the 16 min wave is 7 K and that of the 32 min wave is 5 K. The peak altitudes for each gravity wave and the corresponding value of T' are given in Table 2. The phases are shown in Figure 4b. The phases indicate vertical prorogation with fairly short vertical wavelengths until the waves begin to dissipate in the lower thermosphere. The waves are strongly affected by dissipation by 175 km altitude where the phase variation is transitioning from a nearly linear decrease with altitude indicative of freely propagating waves to altitude independence indicative of strongly dissipating waves.

[31] Figure 5 shows the total wave-induced heating rate (Kelvin day^{-1}) for each acoustic wave in Set 1. The peak heating occurs slightly higher than the T' amplitude peaks, except for the 8 min wave which is double peaked with the upper peak about 50 km above its corresponding T' peak. The amplitude of the heating is ordered like the T' amplitudes. The peak heating for the 4 min wave slightly exceeds 400 K day^{-1}. The heating for the 2 and 1 min waves are, respectively, 280 and 150 K day^{-1}. The heating rate for the 30 s wave is least, with the heating around 70 K day^{-1}. The peak altitudes for each acoustic wave and the corresponding values of Q are given in Table 3.

Table 2. Altitudes at Which the Waves Have Their Maximum Temperature Amplitudes and the Magnitudes of the Temperature Maxima

Period (min)	Horizontal Wavelength (km)	Amplitude of T'_{max} (K)	Altitude of Maximum T' (km)
	Set 1 Acoustic Waves		
0.5	9	2	140
1	18	4	150
2	36	8	160
4	72	11.5	175
8	144	7	200
	Set 1 Gravity Waves		
16	48	7	150
32	96	5	130

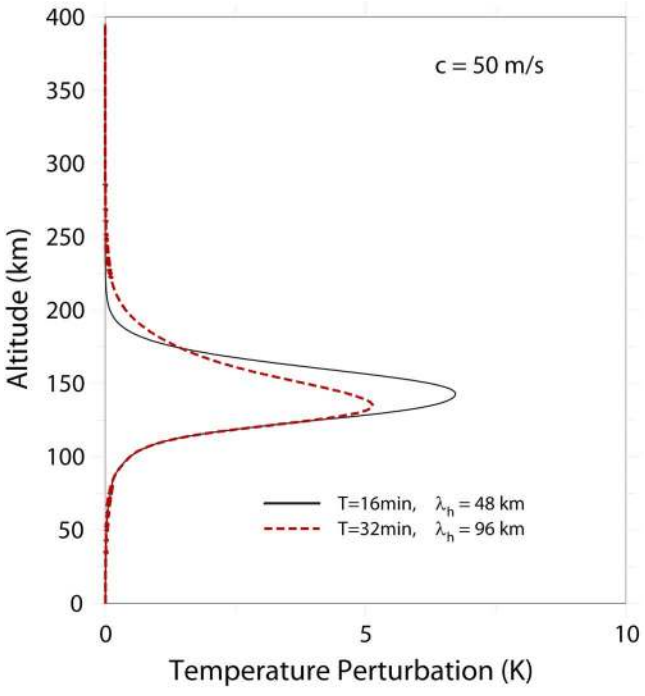

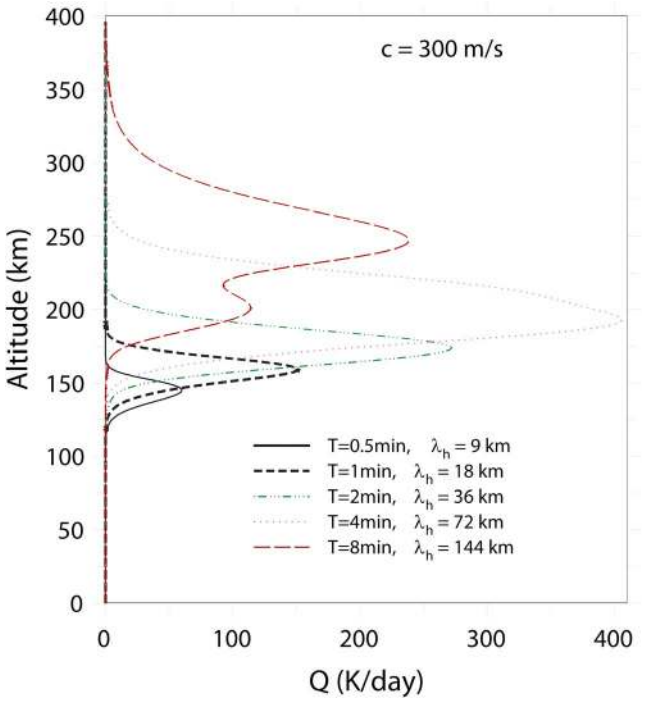

Figure 5. Wave-induced total heating versus altitude for the five Set1 acoustic waves listed in Table 1.

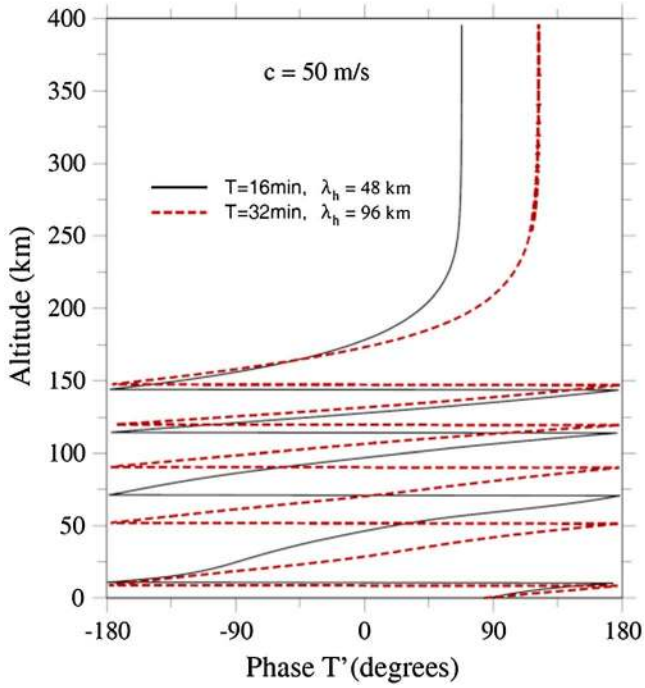

Figure 4. Same as Figure 3, but for the two Set 1 gravity waves listed in Table 1.

[32] The double maximum seen in the results for the 8 min wave is explained by the heating due to the viscous flux of wave kinetic energy (kinetic energy transported by viscosity) that can dominate for waves that reach altitudes where viscous dissipation is extremely large [*Walterscheid and Hickey*, 2011]. See also Figure 7.

[33] Figure 6 shows the total wave-induced heating rate for the two Set 1 gravity waves listed in Table 1. For the gravity waves both heating and cooling are seen, the heating/cooling rates for the 16 min wave being significantly greater than for the 32 min wave. The ordering reflects the relative amplitudes of the two waves. The cooling for both waves peaks near 160 km, with the cooling rate being $-52\,\mathrm{K\,day^{-1}}$ for the 16 min wave and $\sim -11\,\mathrm{K\,day^{-1}}$ for the 32 min wave. The heating for the 16 min wave peaks around 140 km with a rate of $12\,\mathrm{K\,day^{-1}}$; for the 32 min wave heating peaks near 125 km with a rate of $3\,\mathrm{K\,day^{-1}}$. That the cooling is greater than the heating reflects the lower background densities where the cooling occurs. The net density-weighted heating and cooling is small [*Walterscheid*, 1984]. The peak altitudes for each gravity wave and the corresponding value of Q are given in Table 3.

[34] Figure 7 shows altitude profiles of the total wave-induced heating rate for each acoustic wave in Set 2 whose properties are listed in Table 1. The waves in this set propagate higher than those in Set 1 before they are attenuated. They grow to larger amplitudes and peak

Table 3. Altitudes at Which the Waves Have Their Maximum Heating Rates and the Magnitudes of the Maximum Heating Rates[a]

Period (min)	Horizontal Wavelength (km)	Amplitude of Q_{max} Kelvin/day	Altitude of Maximum Q_{max} (km)
		Set 1 Acoustic Waves	
0.5	9	145	60
1	18	160	150
2	36	290	145
4	72	410	180
8	144	230	250
		Set 1 Gravity Waves	
16	48	12/(52)	140/160
32	96	3/(11)	125/160

[a]Parentheses denote cooling.

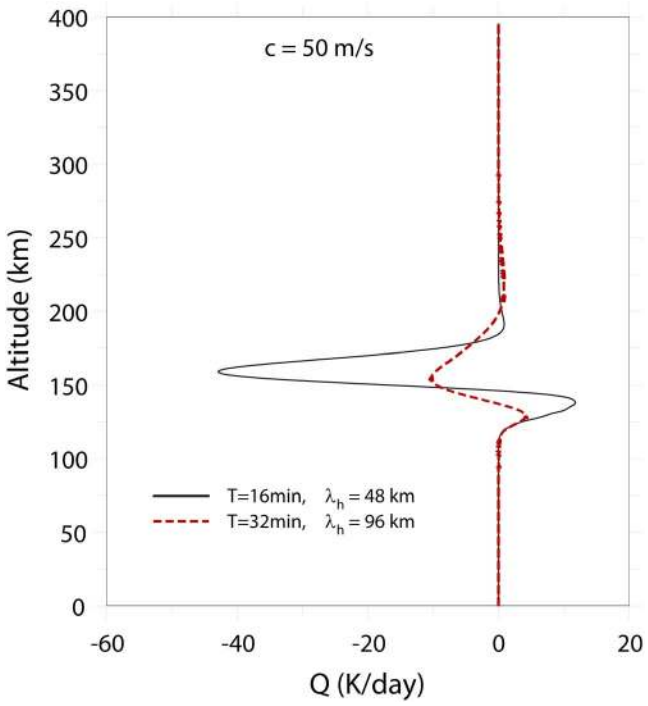

Figure 6. Same as Figure 5 but for the two Set 1 gravity waves in Table 1.

where the background density is lower, and this is reflected in the heating. For the same periods, the heating is about a factor of ~2–3 greater than for the Set 1 waves. The heating peaks about 25 km higher for the three waves with the largest heating rates.

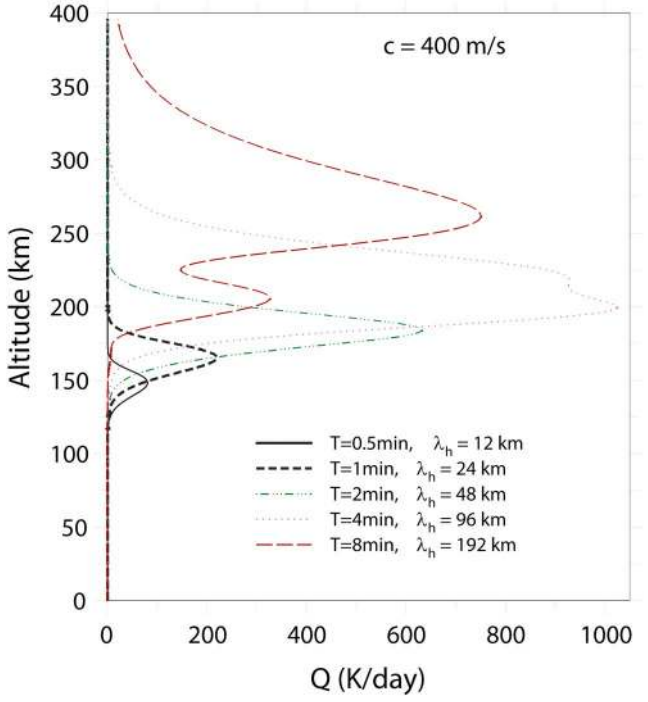

Figure 7. Same as Figure 5 but for the five acoustic waves in Set 2 listed in Table 1.

Table 4. Cycle-Averaged Jeans Escape Flux Relative to Background Flux for Set 1 Waves for Latitude = 45°N and Exobase Height = 219.3 km[a]

Period (min)	Wavelength (km)	Phase Speed (m/s)	T'/T at exobase	$\phi'/\overline{\phi}$ at exobase
0.5	9	300	9.08×10^{-19}	0
1.0	18	300	8.29×10^{-9}	-1.44×10^{-8}
2.0	36	300	1.52×10^{-4}	4.88×10^{-5}
4.0	72	300	8.65×10^{-3}	4.62×10^{-1}
8.0	144	300	1.79×10^{-2}	3.16×10^{0}
16.0	48	50	3.32×10^{-5}	-3.99×10^{-5}
32.0	96	50	4.89×10^{-4}	-6.92×10^{-4}

[a]Also, given are the properties of the waves (wavelength, phase speed, and relative temperature oscillation) at the exobase.

[35] The cycle-averaged Jeans escape flux for the waves in Set 1 (Table 1) evaluated at the exobase (near 220 km) from (9)–(11) is given in Table 4. Only the two waves that have appreciable amplitudes at the exobase have significant values. These are the 4 and the 8 min waves. For the former the wave-induced flux is ~ 50% of the background flux, and for the latter it is ~ 320%, far-exceeding background levels. The cycle-averaged flux for the gravity waves is negligible, because they dissipate far below the exobase.

[36] The cycle-averaged Jeans escape flux for the waves in Set 2 (Table 1) evaluated at the exobase is given in Table 5. The Jeans escape flux for the 4 and 8 min waves has been greatly increased by the fact that the faster waves reach higher altitudes before they are attenuated and thus have greater amplitudes near the exobase. The amplitudes have increased by nearly an order of magnitude.

[37] Only the two waves that have appreciable amplitudes at the exobase have significant values. These are the 4 and the 8 min waves. For the former the wave-induced flux is ~ 1200% of the background flux, and for the latter it is ~ 2900%, thus far-exceeding background levels. The cycle-averaged flux for the gravity waves is negligible, because they dissipate far below the exobase.

[38] We also examined fast gravity waves with a phase speed of 150 m s^{-1} and periods of 16 and 32 min. The 32 min wave is given in Table 1, Set 2 waves. The 16 min wave was evanescent in the lower thermosphere and had neither appreciable amplitude in the upper thermosphere nor any appreciable effect on Jeans escape. The results for the 32 min wave are given in Figure 8 (heating) and Table 5 (Jeans escape flux). The heating in the upper thermosphere is significant with a peak heating of 300 K day^{-1} near 200 km.

Table 5. Cycle-Averaged Jeans Escape Flux Relative to Background Flux for Set 2 Waves for Latitude = 45°N and Exobase Height = 219.3 km[a]

Period (min)	Wavelength (km)	Phase Speed (m/s)	T'/T at exobase	$\phi'/\overline{\phi}$ at exobase
0.5	12	400	4.15×10^{-14}	8.70×10^{-14}
1.0	24	400	1.15×10^{-6}	-3.94×10^{-6}
2.0	48	400	1.65×10^{-3}	1.02×10^{-2}
4.0	96	400	2.66×10^{-2}	1.22×10^{1}
8.0	192	400	3.32×10^{-2}	2.93×10^{1}
32.0	288	150	2.67×10^{-2}	1.23×10^{1}

[a]Also, given are the properties of the waves (wavelength, phase speed, and relative temperature oscillation) at the exobase.

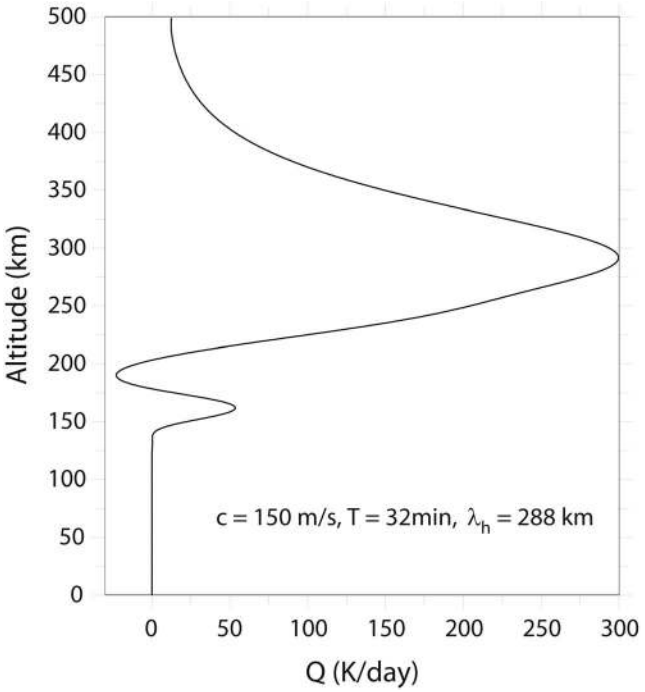

Figure 8. Same as Figure 5 but for the 32 min gravity wave in Set 2 listed in Table 1.

There are comparatively minor regions of heating (cooling) near 160 km (190 km) with rates of 50 K day^{-1} (-40 K day^{-1}). The existence of the added upper region of heating (relatable to the viscous flux of kinetic energy) is a characteristic of fast gravity waves not too far from evanescence [*Hickey et al*., 2011]. Wave-induced Jeans escape is considerable for this wave being on the order of 10 times background.

7. Discussion and Conclusions

[39] We have calculated prodigious heating rates for acoustic waves that reach the exosphere and upper thermosphere. The amplitudes we calculate are consistent with the terrestrial values found for waves launched by gusty flow over rough terrain [*Walterscheid and Hickey*, 2005]. The net effect of the heating will be reduced by intermittency and localization. However, the heating rates suggest that the heating over a geographically extensive area of sources can be quite significant. It has been suggested that wave heating is responsible for the terrestrial "hot spot" located over the Andes [*Meriwether et al*., 1996, 1997; *Walterscheid and Hickey*, 2005]. A similar mechanism might account in good part for the large thermospheric heating that occurs during Martian dust storms [*Lillis et al*., 2008]. This is because during dust storms one expects the generation of acoustic and fast gravity waves by gusty flow over rough terrain to be greatly increased.

[40] Significant heating and cooling rates are found for gravity waves in the thermosphere. Typical waves with phase speeds on the order of tens of meters per second heat and cool the lower thermosphere, while faster waves contribute to heating and cooling of the upper thermosphere. The heating/cooling rates produced by the 50 m s^{-1} wave shown in Figure 6 may be compared with those shown in *Medvedev and Yigit* [2012]. These authors showed heating and cooling rates produced by waves with phase speeds ≤ 60 m s^{-1} for altitudes up to 160 km. The heating rates between 100 and 160 km, where the main contribution is from fast waves, are similar to those for the 16 min, 50 m s^{-1} wave (a few tens of degrees Kelvin).

[41] We have calculated the temperature effects on cycle-averaged, wave-perturbed Jeans flux for the acoustic and gravity waves sets given in Table 1. We find that for acoustic waves with periods of minutes that reach the upper thermosphere with significant amplitudes, the perturbed Jeans flux can far exceed background levels. This occurs because of the exponential dependence of the Jeans flux on temperature. When intermittency and localization are taken into account, wave-induced Jeans flux might not be large compared to the background flux, but our calculations suggest that the wave-induced component may be a significant factor in atmospheric loss.

[42] We have chosen wave amplitudes to be roughly consistent with a dominance of fast waves seen near 125 km altitude in the Mars Global Surveyor and Mars Odyssey data [*Fritts et al*., 2006]. We have diminished the observed amplitudes by 30% and partitioned the remaining energy equally among seven waves, so that each wave has the observed amplitude reduced by a factor of 10. We chose variable frequency and wavelength spacing to give nearly equal contributions to the total root-mean-square amplitude for each period-wavelength bin. This gives thermospheric amplitudes that are roughly consistent with values inferred for waves excited by gusty flow over rough terrain. An alternate approach where wave amplitudes are varied with period and wavelength would give relatively larger waves at longer periods and wavelengths. However, these are the waves that attain greater altitudes with large amplitudes and give the largest heating rates and Jeans escape. In addition, we have not included the effect of perturbation winds or wave-induced heating of the mean state on Jeans escape [*Hartle and Mayr*, 1976]. Thus, we believe that our approach gives relatively conservative estimates of the heating and Jeans escape effects of waves.

[43] The exobase altitude we calculate is significantly greater than values in the range 165 to 195 km calculated by *Valeille et al*. [2009] using the same criterion (where the scale height equals the mean free path). If the exobase were in the middle of the range calculated by *Valeille et al*. [2009], rather than 219 km, then Jeans escape would be very much greater for the 1 and 2 min acoustic waves and much diminished for the slower 4 and 8 min waves.

[44] We have only considered a single basic state profile. However, except possibly for the 50 ms^{-1} wave (which does not play a major role in thermospheric heating or in Jeans escape), we do not expect a dependency on background conditions that would negate the indications of our calculations. The mid-latitude profile that we have chosen is representative of a large range of conditions. The strongest dependency affecting wave propagation should be on winds through the intrinsic frequency (viscous attenuation and evanescence). The waves that contribute most to heating and Jeans escape in the thermosphere are fast waves (speeds of 300–400 m s^{-1}) whose intrinsic frequencies are not unduly sensitive to moderate differences in background winds. The most profound wind effects are at critical levels, and these could be

encountered above 120 km altitude depending on season, latitude, and local time. The Mars Climate Database (http://www-mars.lmd.jussieu.fr) shows that for LS = 270 the northern hemisphere zonal wind variation over longitude at 200 km shows a maximum with speeds of around 300 m s^{-1}, while the meridional wind maximum is around 200 m s^{-1}. Winds away from these maxima are far weaker. Zonally propagating fast waves might encounter a critical level, while waves propagating meridionally or against the wind should avoid critical level absorption. Except to the extent that intrinsic frequency depends on the azimuth of wave propagation, the effects we consider (wave heating and Jeans escape) are independent of the azimuth of propagation. This is in contrast to drag where the azimuth of mean state acceleration is inherently dependent on the azimuth of wave propagation. A fuller study beyond this initial demonstration that fast waves can have large effects on Jeans escape should explore seasonal and latitudinal variations of the basic state and account for the effects of winds.

[45] We conclude that acoustic waves and very fast gravity waves may be a significant source of heating and Jeans escape for the upper thermosphere of Mars.

[46] **Acknowledgments.** Work by R.L.W. on this study was supported by NSF grants AGS1042259 and AGS1001086. Work by M.P.H. was supported by NSF grant AGS-1001074. G.S. was supported by NASA PATM grant NNX11AD67G.

References

Aharonson, O., M. T. Zuber, and D. H. Rothman (2001), Statistics of Mars' topography from the Mars Orbiter Laser Altimeter: Slopes, correlations, and physical Models, *J. Geophys. Res.*, *106*(E10), 23,723–23,735, doi:10.1029/2000JE001403.

Ando, H., T. Imamura, and T. Tsuda (2012), Vertical wavenumber spectra of gravity waves in the Martian atmosphere obtained from Mars Global Surveyor radio occultation data, *J. Atmos. Sci.*, *69*, 2906–2912, doi:10.1175/JAS-D-11-0339.1.

Angelats i Coll, M., F. Forget, M. A. López-Valverde, and F. González-Galindo (2005), The first Mars thermospheric general circulation model: The Martian atmosphere from the ground to 240 km, *Geophys. Res. Lett.*, *32*, L04201, doi:10.1029/2004GL021368.

Creasey, J. E., J. M. Forbes, and D. P. Hinson (2006a), Global and seasonal distribution of gravity wave activity in Mars' lower atmosphere derived from MGS radio occultation data, *Geophys. Res. Lett.*, *33*, L01803, doi:10.1029/2005GL024037.

Creasey, J. E., J. M. Forbes, and G. M. Keating (2006b), Density variability at scales typical of gravity waves observed in Mars' thermosphere by the MGS accelerometer, *Geophys. Res. Lett.*, *33*, L22814, doi:10.1029/2006GL027583.

Eckermann, S. D., J. Mab, and X. Zhu (2011), Scale-dependent infrared radiative damping rates on Mars and their role in the deposition of gravity-wave momentum flux, *Icarus*, *211*, 429–442, doi:10.1016/j.icarus.2010.10.029.

Fenton, L. K., and T. I. Michaels (2010), Characterizing the sensitivity of daytime turbulent activity on Mars with the MRAMS LES: Early results, *Mars*, *5*, 159–171, doi:10.1555/mars.2010.0007.

Forget, F., F. Hourdin, R. Fournier, C. Hourdin, O. Talagrand, M. Collins, S. R. Lewis, P. L. Read, and J.-P. Huot (1999), Improved general circulation models of the Martian atmosphere from the surface to above 80 km, *J. Geophys. Res.*, *104*, 24,155–24,175.

Forget, F., F. Montmessin, J.-L. Bertaux, F. González-Galindo, S. Lebonnois, E. Quemerais, A. Reberac, E. Dimarells, and M. A. Lopez-Valverde (2009), Density and temperatures of the upper Martian atmosphere measured by stellar occultations with Mars Express SPICAM, *J. Geophys. Res.*, *114*, E01004, doi:10.1029/2008JE003086.

Fritts, D. C., and T. J. Dunkerton (1985), Fluxes of heat and constituents due to convectively unstable gravity waves, *J. Atmos. Sci.*, *42*, 549–556.

Fritts, D. C., L. Wang, and R. H. Tolson (2006), Mean and gravity wave structures and variability in the Mars upper atmosphere inferred from Mars Global Surveyor and Mars Odyssey aerobraking densities, *J. Geophys. Res.*, *111*, A12304, doi:10.1029/2006JA011897.

Hartle, R. E., and H. G. Mayr (1976), Wind-enhanced escape with application to terrestrial helium, *J. Geophys. Res.*, *81*(7), 1207–1212, doi:10.1029/JA081i007p01207.

Hecht, J. H., S. K. Ramsay Howat, R. L. Walterscheid, and J. R. Isler (1995), Observations of spectra of intensity fluctuations of the OH Meinel nightglow during ALOHA-93, *Geophys Res. Lett*, *22*, 2873–2876.

Hickey, M. P., R. L. Walterscheid, and G. Schubert (2000), Gravity wave heating and cooling in Jupiter's thermosphere, *Icarus*, *148*(1), 266–81.

Hickey, M. P., G. Schubert, and R. L. Walterscheid (2001), Acoustic wave heating of the thermosphere, *J. Geophys. Res.*, *106*(A10), 21,543–21,548.

Hickey, M. P., R. L. Walterscheid, and G. Schubert (2011), Gravity wave heating and cooling of the thermosphere: Roles of the sensible heat flux and viscous flux of kinetic energy, *J. Geophys. Res.*, *116*, A12326, doi:10.1029/2011JA016792.

Izakov, M. N. (1978), The Martian upper atmosphere structure from the Viking spacecraft experiments, *Icarus*, *36*, 189–197.

Jeans, J. H. (1925), *The Dynamical Theory of Gases*, 4th ed., Cambridge Univ. Press, Cambridge.

Johnson, R. E., M. R. Combi, J. L. Fox, W.-H. Ip, F. Leblanc, M. A. McGrath, V. I. Shematovich, D. F. Strobel, and J. H. Waite Jr. (2008), Exospheres and atmospheric escape, *Space Sci. Rev.*, *139*, 355–397, doi:10.1007/s11214-008-9415-3.

Leovy, C. (2001), Weather and climate on Mars, *Nature*, *412*, 245–249, doi:10.1038/350.

Lewis, S. R., M. Collins, P. L. Read, F. Forget, F. Hourdin, R. Fournier, C. Hourdin, O. Talagrand, and J.-P. Huot (1999), A climate database for Mars, *J. Geophys. Res.*, *104*(E10), 24,177–24,194, doi:10.1029/1999JE001024.

Lillis, R. J., S. W. Bougher, D. L. Mitchell, D. A. Brain, R. P. Lin, and M. H. Acuña (2008), Continuous monitoring of nightside upper thermospheric mass densities in the Martian southern hemisphere over 4 Martian years using electron reflectometry, *Icarus*, *194*, 562–574.

Medvedev, A. S., and E. Yigit (2012), Thermal effects of internal gravity waves in the Martian upper atmosphere, *Geophys. Res. Lett.*, *39*, L05201, doi:10.1029/2012GL050852.

Medvedev, A. S., E. Yiğit, P. Hartogh, and E. Becker (2011), Influence of gravity waves on the Martian atmosphere: General circulation modeling, *J. Geophys. Res.*, *116*, E10004, doi:10.1029/2011JE003848.

Meriwether, J. W., L. Mirick, M. A. Biondi, F. A. Herrero, and C. G. Fesen (1996), Evidence for orographic wave heating in the equatorial thermosphere at solar maximum, *Geophys. Res. Lett.*, *23*, 2177–2180.

Meriwether, J. W., M. A. Biondi, F. A. Herraro, C. G. Fesena, and D. C. Hallenback (1997), Optical interferometric studies of the nighttime equatorial thermosphere: Enhanced temperatures and zonal wind gradients, *J. Geophys. Res.*, *102*, 20,041–20,058.

Miyoshi, Y., J. M. Forbes, and Y. Moudden (2011), A new perspective on gravity waves in the Martian atmosphere: Sources and features, *J. Geophys. Res.*, *116*, E09009, doi:10.1029/2011JE003800.

Orlanski, I., and K. Bryan (1969), Formation of the thermocline step structure by large-amplitude internal gravity waves, *J. Geophys. Res.*, *74*, 6875–6983.

Parish, H. F., G. Schubert, M. P. Hickey, and R. L. Walterscheid (2009), Propagation of tropospheric gravity waves into the upper atmosphere of Mars, *Icarus*, *203*, 28–37, doi:10.1016/j.icarus.2009.04.031.

Schubert, G., M. P. Hickey, and R. L. Walterscheid (2003), Heating of Jupiter's thermosphere by the dissipation of upward propagating acoustic waves, *Icarus*, *163*, 398–413.

Spiga, A., F. González-Galindo, M.-Á. López-Valverde, and F. Forget (2012), Gravity waves, cold pockets and CO_2 clouds in the Martian mesosphere, *Geophys. Res. Lett.*, *39*, L02201, doi:10.1029/2011GL050343.

Strobel, D. F. (1989), Constraints on gravity wave induced diffusion in the middle atmosphere, *Pure Appl. Geophys.*, *130*, 533–546.

Valeille, A., M. R. Combi, S. W. Bougher, V. Tenishev, and A. F. Nagy (2009), Three-dimensional study of Mars upper atmosphere/ionosphere and hot oxygen corona: 2. Solar cycle, seasonal variations, and evolution over history, *J. Geophys. Res.*, *114*, E11006, doi:10.1029/2009JE003389.

VanZandt, T. E. (1982), A universal spectrum of buoyancy waves in the atmosphere, *Geophys. Res. Lett.*, *9*, 575–578.

Walterscheid, R. L. (1981), Dynamical cooling induced by dissipating internal gravity waves, *Geophys. Res. Lett.*, *8*(12), 1235–1238.

Walterscheid, R. L. (1984), Gravity wave attenuation and the evolution of the mean state following wave breakdown, in *Dynamics of the Middle Atmosphere*, edited by J. R. Holton and T. Matsuno, pp. 19–44, Terra Scientific Publishing Co., Tokyo and D. Reidel Publishing Co., Boston.

Walterscheid, R. L., and J. H. Hecht (2003), A reexamination of evanescent acoustic-gravity waves: Special properties and aeronomical significance, *J. Geophys. Res.*, *108*(D11), 4340, doi:10.1029/2002JD002421.

Walterscheid, R. L., and M. P. Hickey (2001), One-gas models with height-dependent mean molecular weight: Effects on gravity wave propagation, *J. Geophys. Res.*, *106*, 28,831–28,839.

Walterscheid, R. L., and M. P. Hickey (2005), Acoustic waves generated by gusty flow over hilly terrain, *J. Geophys. Res.*, *110*, A10307, doi:10.1029/2005JA011166.

Walterscheid, R. L., and M. P. Hickey (2011), Group velocity and energy flux in the thermosphere: Limits on the validity of group velocity in a viscous atmosphere, *J. Geophys. Res.*, *116*, D12101, doi:10.1029/2010JD014987.

Walterscheid, R. L., and G. Schubert (1990), Nonlinear evolution of an upward propagating gravity wave: Overturning, convection, transience and turbulence, *J. Atmos. Sci.*, *47*, 101–125, doi:10.1175/1520-0469(1990)047<0101:NEOAUP>2.0.CO;2.

Walterscheid, R. L., G. Schubert, and D. G. Brinkman (2003), Acoustic waves in the upper mesosphere and lower thermosphere generated by deep tropical convection, *J. Geophys. Res.*, *108*(A11), 1392, doi:10.1029/2003JA010065.